

# Spatio-temporal oscillations and rheochaos in a simple model of shear banding

S. M. Fielding\* and P. D. Olmsted

*Polymer IRC and Department of Physics & Astronomy,  
University of Leeds, Leeds LS2 9JT, United Kingdom*

(Dated: January 26, 2018)

We study a simple model of shear banding in which the flow-induced phase is destabilised by coupling between flow and microstructure (wormlike micellar length). By varying the strength of the instability and the applied shear rate, we find a rich variety of oscillatory and rheochaotic shear banded flows. At low shear and weak instability, the induced phase pulsates in width next to one wall of the flow cell. For stronger instability, single or multiple high shear pulses ricochet across the cell. At high shear rates we observe oscillating bands on either side of a defect. In some cases, multiple such defects exist and propagate across the cell to interact with each other. We discuss our results in the context of recent observations of oscillating and fluctuating shear banded flows.

PACS numbers: 47.50.+d Non-Newtonian fluid flows– 47.20.-k Hydrodynamic stability– 47.54.+j Chaos in fluid mechanics 47.54.+r Pattern selection; pattern formation in fluid mechanics

Complex fluids commonly undergo flow instabilities and flow-induced phase transitions that result in spatially heterogeneous “shear banded” states. Classically studied systems include wormlike micellar surfactants [1]; dense lamellar onion [2] or micellar cubic [3] phases; and polymer solutions [4]. Fluidity banding has also been reported in soft glassy materials [5] such as colloidal suspensions [6] and simulated Lennard Jones particles [7]. Experimentally, the basic observation is of two coexisting shear bands with differing viscosity and microstructure (or fluidity). Theoretically, this is captured by invoking multiple flow branches in the constitutive relation of shear stress *vs.* shear rate,  $\Sigma(\dot{\gamma})$  [8, 9, 10]. The system then separates into a steady state comprising two shear bands, each on its own flow branch (Fig. 1a).

However an accumulating body of data shows this basic picture to be oversimplified: Many shear banding systems display *oscillations* or *irregular fluctuations suggesting chaos* in their bulk rheology, rheo-optics or velocimetry. Example systems include onion phases (at the layering transition [11] or showing size oscillations [12]); wormlike micelles (WMs) with a stress plateau in the flow curve [13]; shear thinning WMs showing common stress banding (band normals in the flow-gradient direction) [14, 15]; shear thickening WMs showing common stress [16] or common strain rate (vorticity) [17] banding; and polymer solutions [4]. In contrast, present models predict steady banded states [8, 9, 10].

In the negligible Reynolds limit relevant to these viscoelastic materials, the non linearity underlying this erratic response must arise in the rheological constitutive behaviour of the system [18]. Temporal “rheochaos” has recently been studied in homogeneous models of director dynamics in sheared nematics [19]; and of shear thickening systems with a single-branched flow curve [18]. In many systems, however, spatial heterogeneity is likely to be a crucial ingredient of rheochaos. In this work, motivated by the above experiments, we introduce the first model of *spatio*-temporal rheochaos in shear banding systems with multi-branched constitutive curves.

Homogeneous flow is unstable in any region of negative constitutive slope,  $d\Sigma/d\dot{\gamma} < 0$ . This is easily seen in models that take the “mechanical variables” ( $\Sigma, \dot{\gamma}$ ) as the relevant dynamic variables [20]. The system can then separate into two shear bands, each on its own stable flow branch. (See Fig. 1a, for shear thinning gradient-banding systems.) In more realistic models, the mechanical variables are coupled to microstructural quantities such as director orientation [8], polymeric concentration [21] or micellar length [22]. This coupling can destabilize the rising high shear branch (causing, *e.g.*, tumbling and wagging in nematics [23]). Here we construct a simple model with an unstable high shear branch (Fig. 1b,c) and show that it has oscillatory and erratic (chaotic) shear banded states at imposed global shear rate. Although we have not yet proved the erratic states to be strictly chaotic, we refer to them as chaotic hereafter. Our model resembles other globally coupled reaction diffusion systems, with similar spatio-temporal behaviour [25]. Aradian and Cates are currently studying spatio-temporal flows of similar models with a single unstable constitutive branch [24].

We use only the minimal ingredients needed to capture the observed phenomena, so do not address the microscopics of any given system. However for concreteness we use the language of shear thinning WMs. There exist numerous reports of apparently unattainable homogeneous high shear rate branches in such systems, in which the sample flows erratically or is ejected from the cell (*e.g.* [1]). This is seldom discussed in detail, but sometimes attributed to surface instability. Nonetheless, the possibility of bulk instability remains. Indeed, in some WMs the high shear band breaks into sub-bands [26].

For simplicity we consider just one microstructural variable, the mean micellar length  $n$ , and define our model by

$$\Sigma = \sigma + \eta\dot{\gamma}, \quad (1)$$

$$\partial_t \sigma = -\frac{\sigma}{\tau(n)} + \frac{g[\dot{\gamma}\tau(n)]}{\tau(n)} + D\partial_y^2 \sigma, \quad (2)$$

$$\partial_t n = -\frac{n}{\tau_n} + \frac{N(\dot{\gamma}\tau_n)}{\tau_n}. \quad (3)$$

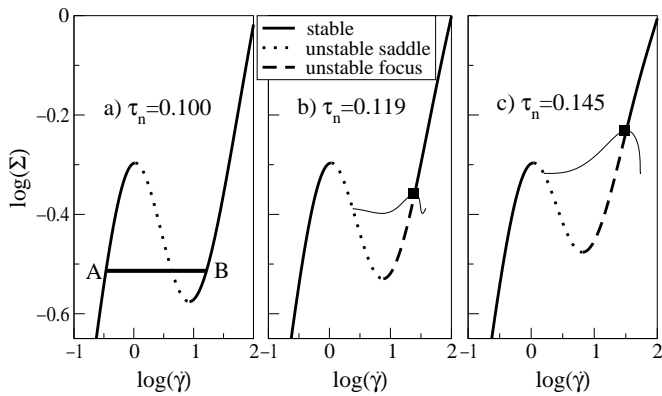


FIG. 1: Intrinsic constitutive curves for differing degrees of coupling between flow and micellar length. a) Weak coupling, giving the standard coexistence of stable low and high shear bands (A and B); b) moderate coupling; c) strong coupling. Squares show Hopf bifurcations. The thin black lines delimit the periodic orbit of the local model at fixed  $\Sigma$ .

Eqn. 1 gives the uniform shear stress  $\Sigma(t)$  in the non-inertial limit. It comprises a (generally non-uniform) viscoelastic micellar contribution  $\sigma(y, t)$  and a solvent contribution with viscosity  $\eta$ . The dynamics of  $\sigma$  (Eqn. 2) has a length-dependent relaxation time [27]

$$\tau(n) = \tau_0 \left( \frac{n}{n_0} \right)^\alpha, \quad (4)$$

and a steady homogeneous state  $\sigma = g[\dot{\gamma}\tau(n)]$  set by

$$g(x) = \frac{x}{1+x^2}, \quad (5)$$

admitting a constitutive curve of negative slope. The spatial gradients  $D\partial_y^2\sigma$  allow for a smooth interface of width  $l \propto \sqrt{D}$  between the shear bands.

The micellar length  $n$  has its own relaxation time  $\tau_n$  (Eqn. 3), presumably related to the (unknown) underlying rates of micellar scission and recombination. For example, scission could be enhanced by the agitation of shearing; or recombination aided by shear-induced alignment of micellar ends [22]. We assume the former, taking

$$N(x) = \frac{n_0}{1+x^\beta}. \quad (6)$$

Because this decrease in length only becomes important for typical shear rates  $\dot{\gamma} > 1/\tau_n$ , the strength of coupling between the mechanical quantities ( $\Sigma, \sigma, \dot{\gamma}$ ) and microstructure  $n$  can be tuned by varying  $\tau_n$ .

Using this model we study flow between two parallel plates at  $y = 0, L$  with boundary condition  $\partial_y \Sigma = 0$ , using units in which  $n_0 = 1, \tau_0 = 1$  and  $L = 1$ . We set  $\alpha = 1.2, \beta = 1.5$ , though our results are qualitatively robust to reasonable variations in these values.

*Homogeneous dynamics*— The constitutive curves  $\Sigma(\dot{\gamma})$  and domains of instability for homogeneous states

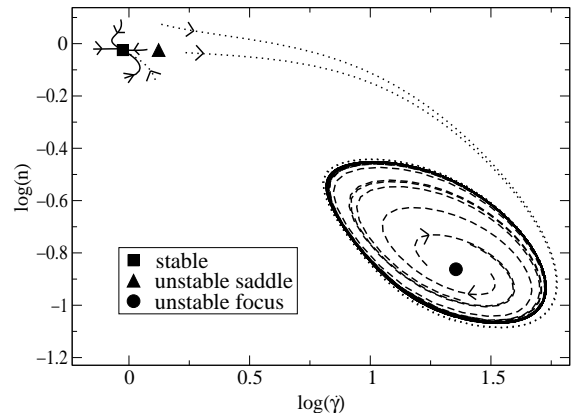


FIG. 2: Homogeneous dynamics ( $D = 0$ ) at fixed  $\log \Sigma = -0.301$  for different initial conditions.  $\tau_n = 0.145$ .

are shown in Fig. 1. For small  $\tau_n \lesssim 0.115$  we find pure mechanical instability (Fig. 1a) that does not involve  $n$ . The constitutive curve is then (at any fixed  $\Sigma$ ) an unstable saddle [28] (one unstable eigenvector). For larger  $\tau_n$ , coupling to micellar length broadens this instability into the rising high shear branch, which is now an unstable focus [28] (two unstable eigenvectors): Fig. 1b,c. This instability terminates in a Hopf bifurcation [28].

We then studied the non-linear dynamics of the local ( $D = 0$ ) model for fixed  $\Sigma$ , solving Eqns. (1-3) via a fourth order Runge-Kutte method [29]. This confirmed the stability properties of Fig. 1: states near an unstable (stable) segment of the constitutive curve flow away from (towards) that segment (Fig. 2). They also reveal a periodic orbit about the unstable high shear branch for stresses just below the Hopf bifurcation. We also used AUTO [30] to trace the amplitude of the periodic orbits, Fig. 1b,c. Periodic orbits are the most complex behaviour possible for the local model since it has only two degrees of freedom,  $d = 2$ . Chaos requires  $d \geq 3$  [28].

*Spatially heterogeneous dynamics*— We now turn to the non-local model,  $D \neq 0$ , focusing on the implications of an unstable high shear branch (Fig. 1b,c). The dimensionality  $d$  is now effectively infinite, since each spatial point has its own value of  $n$  and  $\dot{\gamma}$ . We solved the non-local equations using a Crank-Nicholson algorithm (checking our results with the Rosenbrock method) [29], with the constraint of fixed global strain rate,  $\bar{\dot{\gamma}} = \int_0^1 dy \dot{\gamma}(y, t)$ . For small  $\tau_n \lesssim 0.115$  we find stable shear bands (Fig. 1a). In contrast for  $\tau_n = 0.145$  (unstable high shear branch) we find spatio-temporal oscillations and chaotic banding flows (Fig. 3).

Several regimes are evident. At low applied shear,  $\bar{\dot{\gamma}} = 1.5$ , a thin pulse of high shear ricochets back and forth across the cell (Fig. 3, top). A thin fluctuating high shear band, away from the rheometer wall, was seen experimentally in Ref. [14]. At larger shear rates, we find two or more such pulses. For two pulses (not shown), we typically find a periodically repeating movie with the pulses alternately bouncing off each other (mid-cell) and

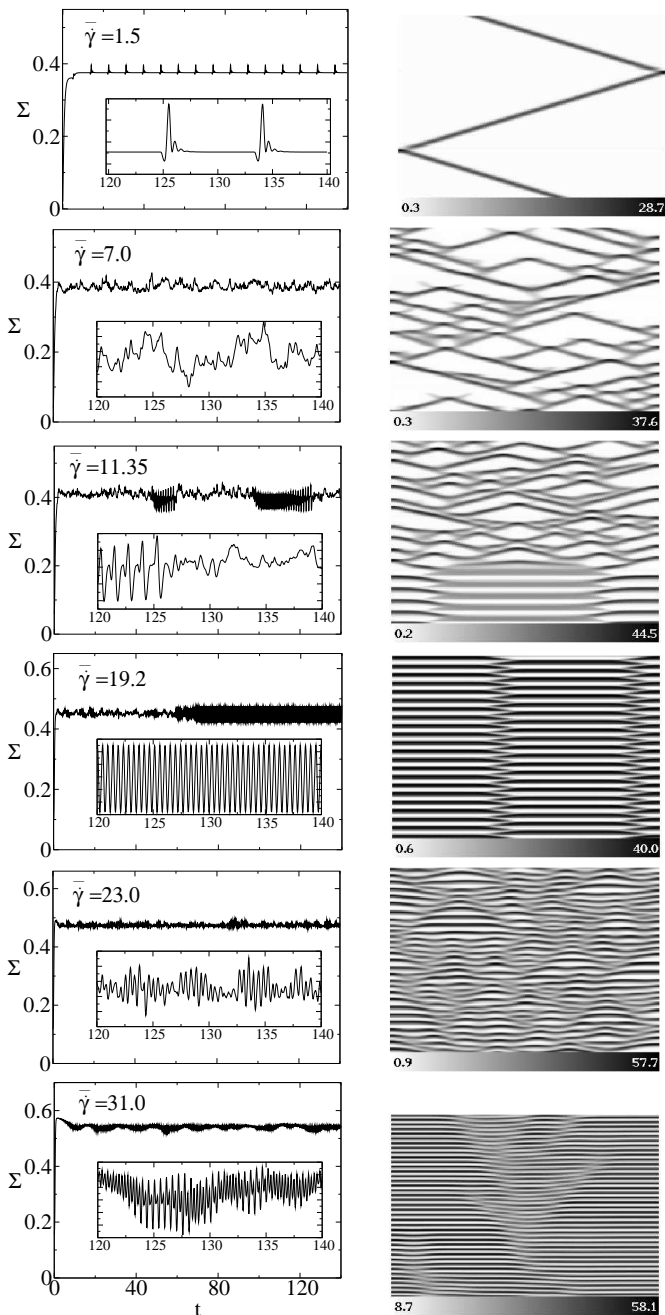


FIG. 3: Right: space time plots for shear rate evolution for  $\tau_n = 0.145$ ,  $D = 0.0016$  with space  $y = 0 - 1$  left-right and time  $t = 120 - 140$  bottom-top. Greyscale for the shear rate is shown in each case. Left: corresponding stress *vs.* time.

the cell walls. Once three pulses are present,  $\bar{\gamma} = 7.0$ , periodicity gives way to chaotic behaviour (Fig. 3).

At still higher shear,  $\bar{\gamma} = 19.2$ , we find regular oscillations of spatially extended bands pinned at a stationary defect. The local shear rates span both the low and high shear constitutive branches. Oscillating (vorticity) bands were seen experimentally in Ref. [4, 17]. For the intermediate value  $\bar{\gamma} = 11.35$  we find intermittency between

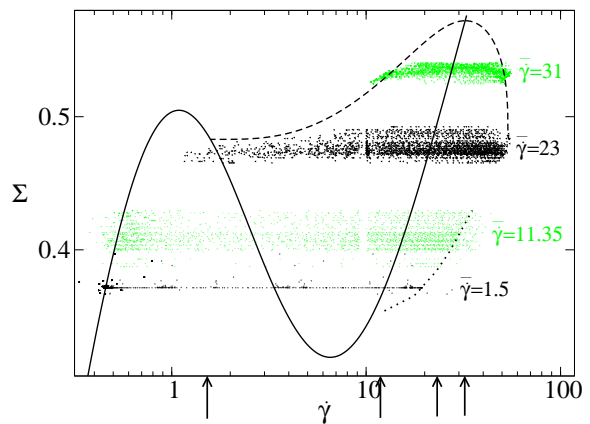


FIG. 4: Space-time data of Fig. 3 for  $\bar{\gamma} = 1.5, 11.35, 23.0, 31.0$  (arrows under abscissa) and  $130 < t < 140$  in condensed form. Solid line – intrinsic constitutive curve; long dashed line – extrema of the periodic orbits of the local model; dotted line – maximum shear rate of the propagating high shear pulse described by Eqns. 8.

patterns resembling those for  $\bar{\gamma} = 7.0$  and  $\bar{\gamma} = 19.2$ .

Finally for  $\bar{\gamma} = 23.0, 31.0$  we find oscillating bands separated by *moving* defects (Fig. 3, bottom right) with the flow now governed only by the high shear constitutive branch. In each band, the shear rate cycles round the periodic orbit of the local model (Fig. 2 and top data set of Fig. 4).

For different values of  $\tau_n$  we find a host of other interesting phenomena [31]. For example, for weaker instability ( $\tau_n = 0.13$ ) at low applied shear rates we see a high shear band that can pulsate in width while adhering to the rheometer wall (Fig. 5a), or meander about the cell (Fig. 5b). The former behaviour resembles interfacial motion in seen WMs [15, 16] and onion phases [11].

Finally we discuss in more detail the high shear pulse of Fig. 3 (top right). At times when the pulse is far from the wall, the stress  $\Sigma$  is constant (flat regions in Fig. 3, top left). In this regime we transform to the pulse’s comoving frame  $\hat{y} = y - ct$  and eliminate  $\sigma$  to get

$$c\eta\dot{\gamma}' = -\frac{\Sigma}{\tau(n)} + \frac{g[\dot{\gamma}\tau(n)] + \eta\dot{\gamma}}{\tau(n)} - D\eta\dot{\gamma}'' \quad (7)$$

$$-cn' = -\frac{n}{\tau_n} + \frac{N(\dot{\gamma}\tau_n)}{\tau_n} \quad (8)$$

in the  $3d$  space  $(n, \dot{\gamma}, \dot{\gamma}')$ , with parameters  $\Sigma$  and  $c$ . (Prime denotes  $\partial/\partial\hat{y}$ .) The low shear regions in Fig. 3 (top right) lie on the low shear branch of the constitutive curve. Although this is a stable stationary flow branch (Fig. 1), in the space of  $(n, \dot{\gamma}, \dot{\gamma}')$  it is actually a fixed point ( $P$ ) with one unstable eigenvector and two stable ones. As  $\hat{y}$  increases through the high shear pulse, the solution’s trajectory moves away from  $P$  along the unstable direction and then back to  $P$  in the stable plane, completing a “homoclinic connection” [28]. The requirement for this  $1d$  trajectory to correctly rejoin the  $2d$  stable manifold selects (for a given  $\Sigma$ ) the observed prop-

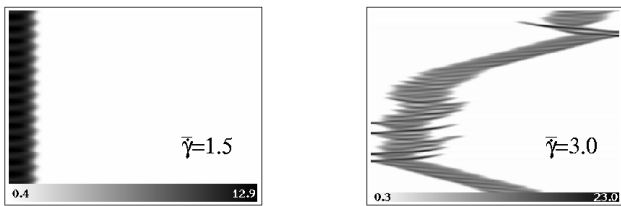


FIG. 5: Shear rate density plots for  $\tau_n = 0.13$ ,  $D = 0.0016$ .

agation speed,  $c$ . For other values of  $c$ , the trajectory abruptly crosses the  $2d$  manifold, missing  $P$ . (This follows by simple dimension counting [10].) Once selected, the solution's profile  $\hat{\gamma}(\hat{y})$  can (for a given value of  $D$ ) be integrated over  $\hat{y}$  to find the globally applied shear rate  $\bar{\gamma}$ . By the reverse reasoning, we find a selected  $\Sigma$  and  $c$  for any  $\bar{\gamma}$  (and  $D$ ). We used AUTO [30] to check that the homoclinic connections of Eqn. 8 indeed coincide with our numerical results. The locus of the maxima  $\hat{\gamma}_h(\Sigma)$  of these connections is marked in Fig. 4. The space-time

points for  $\hat{\gamma} > \hat{\gamma}_h$  arise during wall collisions; correspondingly, their density is smaller than for  $\hat{\gamma} < \hat{\gamma}_h$ .

To summarise, we have constructed a simple model of shear banding in which the high shear branch of the underlying constitutive curve is rendered unstable by a coupling between flow and microstructure. Within this model, we have found a rich variety of spatio-temporal oscillatory and rheochaotic flows, many resembling experimental observations in shear banding systems. It remains an open challenge to delineate more fully the spectrum of mechanisms governing rheochaotic banded states. Extension to higher dimensions, allowing fluctuations along the plane of the interface would be interesting. Within the present one-dimensional approach, generalisation to shear thickening systems [24], curved Couette geometries and vorticity-banding is underway [31].

We thank A. A. Aradian, P. T. Callaghan, M. E. Cates, E. Knobloch, A. M. Rucklidge and J.-B. Salmon for interesting discussions; and EPSRC GR/N11735 for funding.

\* Electronic address: s.m.fielding@leeds.ac.uk

- [1] M. M. Britton and P. T. Callaghan, Phys. Rev. Lett. **78**, 4930 (1997). J. F. Berret, G. Porte, and J. P. Decruppe, Phys. Rev. **E 55**, 1668 (1997). V. Schmitt, F. Lequeux, A. Pousse, and D. Roux, Langmuir **10**, 955 (1994).
- [2] O. Diat, D. Roux, and F. Nallet, J. Phys. II (France) **3**, 1427 (1993).
- [3] E. Eiser, F. Molino, G. Porte, and O. Diat, Phys. Rev. E **61**, 6759 (2000).
- [4] L. Hilliou and D. Vlassopoulos, Ind. Eng. Chem. Res. **41**, 6246 (2002).
- [5] P. Sollich, F. Lequeux, P. Hébraud, and M. E. Cates, Phys. Rev. Lett. **78**, 2020 (1997);
- [6] J. S. Raynaud, P. Moucheron, J. C. Baudez, F. Bertrand, J. P. Guilbaud, and P. Coussot, J. Rheol. **46**, 709 (2002).
- [7] F. Varnik, L. Bocquet, J. L. Barrat, and L. Berthier, Phys. Rev. Lett. **90**, 095702 (2003).
- [8] P. D. Olmsted and P. M. Goldbart, Phys. Rev. **A41**, 4578 (1990); *ibid* **A46**, 4966 (1992).
- [9] N. A. Spenley, M. E. Cates, and T. C. B. McLeish, Phys. Rev. Lett. **71**, 939 (1993).
- [10] C.-Y. D. Lu, P. D. Olmsted, and R. C. Ball, Phys. Rev. Lett. **84**, 642 (2000).
- [11] J. B. Salmon, A. Colin, and D. Roux, Phys. Rev. E **66**, 031505 (2002); J.-B. Salmon, S. Manneville, and A. Colin, Pre-print cond-mat/0307609.
- [12] L. Courbin, P. Panizza, and J.-B. Salmon, Pre-print cond-mat/0303225.
- [13] R. Bandyopadhyay, G. Basappa, and A. K. Sood, Phys. Rev. Lett. **84**, 2022 (2000).
- [14] W. M. Holmes, M. R. López-González, and P. T. Callaghan, Europhys. Lett. **64**, 274 (2003).
- [15] M. M. Britton and P. T. Callaghan, Eur. Phys. J. B **7**, 237 (1999).
- [16] Y. T. Hu, P. Boltenhagen, and D. J. Pine, J. Rheol. **42**, 1185 (1998). R. Bandyopadhyay and A. K. Sood, Europhys. Lett. **56**, 447 (2001)
- [17] P. Fischer, E. K. Wheeler, and G. G. Fuller, Rheol. Acta **41**, 35 (2002).
- [18] M. E. Cates, D. A. Head, and A. Ajdari, Phys. Rev. E **66**, 025202 (2002).
- [19] M. Grosso, R. Keunings, S. Crescitelli, and P. L. Maffettone, Phys. Rev. Lett. **86**, 3184 (2001); G. Rienacker, A. Kroger, and S. Hess, Phys. Rev. E **66**, 040702 (2002).
- [20] J. Yerushalmi, S. Katz, and R. Shinnar, Chemical Engineering Science **25**, 1891 (1970).
- [21] S. M. Fielding and P. D. Olmsted, Eur. Phys. J. E **11**, 65 (2003); Phys. Rev. Lett. **90**, 224501 (2003).
- [22] M. E. Cates and M. S. Turner, J. Phys. Cond. Matt. **4**, 3719 (1992).
- [23] M. Doi, J. Poly. Sci: Poly. Phys. **19**, 229 (1981); R. G. Larson, Macromolecules **23**, 3983 (1990). M. Grosso, S. Crescitelli, E. Somma, J. Vermant, P. Moldenaers, and P. L. Maffettone, Phys. Rev. Lett. **90**, 098304 (2003).
- [24] A. A. Aradian and M. E. Cates. Preprint cond-mat/0310660.
- [25] M. Kim, M. Bertram, M. Pollmann, A. von Oertzen, A. S. von Mikhailov, H. H. Rotermund, and G. Ertl, Science. **292**, 1357 (2001).
- [26] S. Lerouge, J. P. Decruppe, and J. F. Berret, Langmuir **16**, 6464 (2000).
- [27] F. Bautista, J. F. A Soltero, J. H. Perez-Lopez, J. E. Puig, and O. Manero, J. Non-Newt. Fl. Mech., **94**, 57 (2000).
- [28] S. H. Strogatz, *Nonlinear dynamics and chaos: with applications to physics, biology, chemistry and engineering* (Addison-Wesley, Reading, MA, 1994).
- [29] W. H. Press, S. A. Teukolsky, W. T. Vetterling, and B. P. Flannery, *Numerical Recipes in C (2nd ed.)* (Cambridge University Press, Cambridge, 1992).
- [30] E. J. Doedel, *AUTO97: continuation and bifurcation software for ordinary differential equations* (Concordia State University, Montreal, 1997).
- [31] S. M. Fielding and P. D. Olmsted. In preparation.